Modern Physics Letters B
(2025) 2550146 (22 pages)

DOI: 10.1142/S0217984925501465

Chemical response in Oldroyd-B liquid through rotational disk with temperature and space-related heat rise

M. Rupa Lavanya [*,¶], Kotha Gangadhar [†,‖], D. Naga Bhargavi [‡,**]
and Ali J. Chamkha [§,††]

[*]*Department of Mathematics, DVR & Dr HS MIC College of Technology, Kanchikacherla, Andhra Pradesh, India*

[†]*Department of Mathematics, AcharyaNagarjuna University, Guntur, Andhra Pradesh 522510, India*

[‡]*Department of Mathematics, Vignan's Nirula Institute of Technology and Science for Women, Palakaluru, Guntur, Andhra Pradesh 522009, India*

[§]*Faculty of Engineering, Kuwait College of Science and Technology, Doha District 35004, Kuwait*
[¶]*lavanyarupa3@gmail.com*
[‖]*kgangadharmaths@gmail.com*
[**]*hasini.d1984@gmail.com*
[††]*a.chamkha@kcst.edu.kw*

Received 16 September 2024
Revised 26 October 2024
Accepted 22 December 2024
Published 29 March 2025

This paper considered the magnetized flow of an Oldroyd-B fluid over a rotational disk. In this investigation, the altered Fourier's law rather than the classic Fourier's law of consideration was used by the fluid thermal features. Its effect on homogeneous–heterogeneous reactions about mass transport was studied. Additionally, interesting characteristics of thermal radiation with temperature and space-related heat sources or sinks were examined. The von Karman variables were utilized to discipline the PDEs toward non-dimensional ODEs. An efficient finite element method was utilized in acquiring the numerical results. The correlation table was invented in an indentured case to save the efficacy of their numerical outcomes in the previous results. It was noticed that the fluid velocity decreases to make an effect on the relaxation time parameter. The thermal distribution on Oldroyd-B fluid displays the diminishing trend on acceleration on the range of thermal relaxation heat flux parameter. Further, higher values of heat generation parameter decline the rate of heat transfer. Furthermore, the absorption rate of the fluid deteriorates a greater strength of the homogeneous reaction.

Keywords: Modified Fourier's law; Oldroyd-B fluid model; heat rise/fall; FEM; homogeneous–heterogeneous response.

PACS Nos.: 02.70.−c, 02.60.Cb, 02.70.Jn

[‖]Corresponding author.

1. Introduction

The well-excited investigation field on fluid mechanics was possibly a rotating disk geometry as a result of those immature common functions in engineering and industry, including electric-power generation turbine systems, centrifugal filtration, jet motors and hard disks. Given the reasoning, this feature of fluid flow through the spinning disk had been intended for massive absorption and was primarily noted by numerous researchers later on in the background separation study of von Karman's flow by ethics on the revolving disk. This extreme motive on the current analysis was to consider the motion of fluid of the Oldroyd-B fluid model into the space on both rotational disks utilizing the novel aspect of the theory of non-Fourier composed into the circumstance of homogeneous–heterogeneous chemical reactions.

The basic analysis of fluid flow by the enormous rotating disk was examined by Karman.[1] Cochran[2] applied transformations of von Karman on time independence in the fluid flow. This accurate result about transient flow previous to the rotating disk was analyzed by Benton.[3] Hafeez *et al.*[4] analyzed the magnetized flow of a viscoelastic fluid about the rotating disk. This bioconvection in Oldroyd-B nanoliquid flow through the vertical stretched sheet into an inclined magnetic field and mixed convection was discussed by Elanchezhian *et al.*[5] Usman *et al.*[6] inspected the authority on uniform less heat rise or sink on the transfer of heat phenomenon to power-law fluid within dual stretchable disks. Their results indicated that temperature increase includes the analogy variable in raising heat source/sink parameters. Alharbi[7] presented the numerical simulation for the transport mechanism of Carreau fluid through the non-uniformly exciting surface.

The circumstance of heat transfer is a very familiar natural phenomenon, and it appears as a result of thermal variation among the substance or contrasting divisions on a similar body. Many researchers have analyzed the circumstances and presence. The classic law on heat conduction by Fourier[8] was fundamental in considering the heat transfer characteristics in various conditions. Also, the main defect of that law was the improvement of the parabolic energy equation stated to be the primary disturbance that was directly concerned with the structure mentioned below. In this paper, the feature is considered physically unrealistic, and it is known as the paradox of heat conduction. That position was observed by numerous investigators by tending the adjustment on Fourier's law. The change of Fourier's imitation by the recommended flux of relaxation time heat was studied by Cattaneo.[9] They were noticed to like conversion return hyperbolic energy equation and that charter of motion by heat breeding on thermal waves over limited speed. Cattaneo's conversion was later enhanced by Christov[10] over the announced time for thermal relaxation in Oldroyd's above-connected results about the material's invariable formation. In this paper, the modification was called as Cattaneo–Christov flux for the heat model. This singularity conducted the result of Cattaneo–Christov equation that was confirmed by Ciarletta and Straughan.[11] Zhang *et al.*[12] investigated analytically the problem of combined buoyant convective transport by nanofluid on annular geometry with Cattaneo law of thermal flux. They investigated that temperature reduces the thermal memory parameter in the area near the exterior wall. Unsteady bidirectional flow on the Newtonian fluid of Cattaneo–Christov dual diffusion is inspected by Ahmad *et al.*[13] Alsharif *et al.*[14] scrutinized the unsteady electroosmotic flow on the compressed fractional second-level fluid through the microchannel.

Of late, engineers and scientists have been concerned about issues concerning the flows of fluids incorporated into chemical responses. The chemical responses can be homogeneous or heterogeneous. In the case of the response increase into the complete domain to a reaction called a homogeneous reaction, as long as the reaction responds interior to a few particular fields or into the boundary on the field, it can be a heterogeneous reaction. Homogeneous–heterogeneous reactions play an important role in various chemically active structures. It was substantial to record the few reactions that developed in a very less rapid manner and few of them did not proceed at all, outside the presence of the motivation. The change of chemical reactions endures, and some of them had important applications in chemical engineering systems and industries. Especially, chemical reactions had a continuous impact on food dispensation, the production of polymers, the hydrometallurgical industry, the chemically designed equipment, ceramics manufacturing and spinney on different crops and tree destruction through freezing. Several researchers used homogeneous–heterogeneous reactions in our analysis to examine various types of flow phenomena. Earlier, Chaudhary and Merkin[15] researched on finding an easy method by working in a homogeneous–heterogeneous response near the stagnation point. Furthermore, Merkin[16] was numerically marked by a boundary layer flow as used by the homogeneous–heterogeneous response. Turkyilmazoglu[17] modeled the heat transfer of nanofluid flow with a spinning disk. Bachok *et al.*[18] performed the features of heat transfer through the spinning porous disk. This effect on homogeneous and heterogeneous response of the heat transfer and the flow study in Maxwell nanofluid with velocity slip was investigated by Sreedevi *et al.*[19] Javed *et al.*[20] deliberated an analysis on the impact of the homogeneous–heterogeneous response of the MHD peristaltic mechanism by the arched medium. Almaneea[21] studied a numerically used finite element method to resolve the problem of heat transport mechanism on Williamson fluid during homogeneous–heterogeneous reactions. Siddiqui *et al.*[22] marked the performance of 3D flow nanofluid and entropy generation along a stretching cylinder. Khashi'ie *et al.*[23] presented an analysis of radiative three-dimensional hybrid nanofluid previous permeable shrinking/stretching sheet. Aladdin and Bachok[24] explored the impact of chemical reaction and hydromagnetic through the stagnation-point flow on horizontal shrinking/stretching cylindrical surfaces.

The consequence of radiation on convective flows shows the extensive act on space technology and more industrial methods requiring greater temperatures, like the preparation of paper plates, petroleum pumps and electric chips. Anantha Kumar *et al.*[25] explored the transferring heat and liquid film flow of hybrid ferrofluid with an irregular heat sink. Rauf *et al.*[26] deliberated an analysis of Casson hybrid nanofluid flow over the lubricated surface on a stagnation point with a uniform magnetic field.

Luo *et al.*[27] presented the active current conductivity of porous constituents on the attendance of thermal radiation. Rana *et al.*[28] conducted the time-dependent improved heat transport in the flow of hybrid nanofluid by the circling sphere. This stagnation in the point flow by Casson nanofluid into thermal radiations was examined by Hussain *et al.*[29] They investigated that the temperature profile improves in developing heat generation parameters. Sharma *et al.*[30] investigated the mass and heat transfer of magnetic nanofluid flow over the turning disk in variable fluid prospects. The mass transfer analysis on ferrofluid flow among co-spinning stretchable disks in geothermal viscosity was carried out by Vijay and Sharma.[31] Kumar and Sharma[32] discussed the entropy-optimized Cu–TiO_2/water flow over a vertically moving rotating disk. Gangadhar *et al.*[33] inspected the bioconvective motion in the MHD flow of the couple stress fluids through the above horizontal surface. Zainal *et al.*[34] presented the unsteady flow of the absorptive shrinking or stretched Riga plate with thermal radiation. The best applicable schedule in the topic can be found in Refs. 35–40.

Influenced by the formal reports, the notable MHD viscoelastic fluid flow over the rotating disk in the effect of space and temperature-related heat source/fall to the fluid has not been investigated yet. Also, the above convected Oldroyd-B fluid figure and the changed Fourier law are utilized to analyze temperature transport and the fluid flow act. Further, we examined the appearance of mass transfer as a working effect on homogeneous–heterogeneous response on the flow of Oldroyd-B fluid that was acquired over the spinning disk. The nonlinear PDEs were transformed with non-dimensional ODEs by applying von Karman transformations[1] to achieve the results. A numerical scheme finite element method gives complete details regarding the investigation of the physical behavior of elaborate parameters in flow, solutal distributions and temperature. The goal of this analysis was achieved through the following questions.

(1) Which relaxation time parameters influence the fluid velocity by azimuthal and radial directions?
(2) What was the importance of radiation and thermal relaxation parameters on the rate of heat transfer and the fluid temperature?
(3) How do homogeneous–heterogeneous reactions move fluid concentration and wall concentration gradient?
(4) What was the effect of Cattaneo–Christov flux for heat by the Oldroyd-B fluid flow?
(5) What was the effect on the heat rise/fall of the heat transfer rate?

2. Mathematical Formulation

We accept the constant incompressible magnetic flow of Oldroyd-B fluid through the rotational disk. This rotation, including radial stretching by the disk, is studied to achieve the flow. This disk was rotating into the fixed angular velocity Ω. This magnetic model behaves in the z_0-direction and the persuaded magnetic model was not studied. Moreover, the effect on homogeneous–heterogeneous response to mass transport was studied in that analysis. The theory of Catteneo–Christov heat flux (changed Fourier's law) was utilized to achieve the heat transport mechanism. Furthermore, the heat transfer investigation was directed into the effect on linear radiation and space and temperature-dependent heat absorption or generation. Figure 1 displays the physical representation of the problem.

Merkin[16] proposed the figure about the homogeneous and heterogeneous response to both chemical species A_1^* and A_2^*. They accepted the homogeneous reaction of the cubic autocatalytic that was given by

$$A_1^* + 2A_2^* \to 3A_2^*; \quad \text{rate} = k_c ab^2. \tag{1}$$

In the catalyst surface, they have the isothermal, single, first-order response which is as follows:

$$A_1^* \to A_2^*; \quad \text{rate} = k_s a. \tag{2}$$

Here, a is the concentration on A_1^* and A_2^* by b and (k_c and k_s) are the rate constants. The abovementioned reactions were studied taking into account an isothermal.

These nonlinear equations of the taken problem are as follows[4,5]:

Conservation of mass

$$\frac{\partial u_0}{\partial r_0} + \frac{1}{r_0} u_0 + \frac{\partial w_0}{\partial z_0} = 0. \tag{3}$$

The momentum equation along the r-direction is as follows:

$$u_0 \frac{\partial u_0}{\partial r_0} - \frac{1}{r_0} v_0^2 + w_0 \frac{\partial u_0}{\partial z_0} = \upsilon \frac{\partial^2 u_0}{\partial z_0^2} - \frac{\sigma}{\rho} B_0^2 \left[u_0 + \lambda_1 w_0 \frac{\partial u_0}{\partial z_0} \right]$$

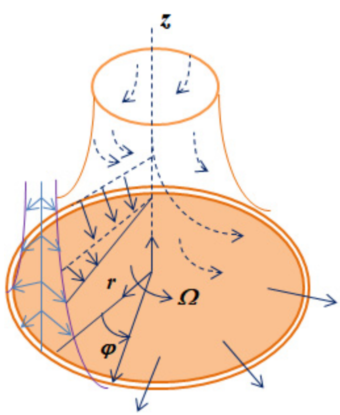

Fig. 1. (Color online) A physical diagram.

$$
-\lambda_1\left[\begin{array}{l} u_0^2\dfrac{\partial^2 u_0}{\partial r_0^2}+w_0^2\dfrac{\partial^2 u_0}{\partial z_0^2}+2u_0w_0\dfrac{\partial^2 u_0}{\partial r_0 z_0}-\dfrac{2}{r_0}u_0v_0\dfrac{\partial v_0}{\partial r_0} \\ \quad -\dfrac{2}{r_0}u_0w_0\dfrac{\partial v_0}{\partial z_0}+\dfrac{1}{r_0^2}u_0v_0^2+\dfrac{1}{r_0}v_0^2\dfrac{\partial u_0}{\partial r_0} \end{array}\right]
+\upsilon\lambda_2\left[\begin{array}{l} -\dfrac{1}{r_0}\left(\dfrac{\partial u_0}{\partial z_0}\right)^2-2\dfrac{\partial u_0}{\partial z_0}\dfrac{\partial^2 w_0}{\partial z_0^2}+w_0\dfrac{\partial^3 u_0}{\partial z_0^3} \\ \quad -\dfrac{\partial u_0}{\partial r_0}\dfrac{\partial^2 u_0}{\partial z_0^2}-\dfrac{\partial u_0}{\partial z_0}\dfrac{\partial^2 u_0}{\partial r_0\partial z_0}+u_0\dfrac{\partial^3 u_0}{\partial r_0\partial z_0^2} \end{array}\right]. \tag{4}
$$

The momentum equation along the s-direction is as follows:

$$
u_0\frac{\partial v_0}{\partial r_0}+\frac{1}{r_0}u_0v_0+w_0\frac{\partial v_0}{\partial z_0}=\upsilon\frac{\partial^2 v_0}{\partial z_0^2}-\frac{\sigma}{\rho}B_0^2\left[v_0+\lambda_1 w_0\frac{\partial v_0}{\partial z_0}\right]
-\lambda_1\left[\begin{array}{l} u_0^2\dfrac{\partial^2 v_0}{\partial r_0^2}+w_0^2\dfrac{\partial^2 v_0}{\partial z_0^2}+2u_0w_0\dfrac{\partial^2 v_0}{\partial r_0 z_0}+\dfrac{2}{r_0}u_0v_0\dfrac{\partial u_0}{\partial r_0} \\ \quad +\dfrac{2}{r_0}u_0w_0\dfrac{\partial u_0}{\partial z_0}-\dfrac{2}{r_0^2}u_0^2v_0-\dfrac{1}{r_0^2}v_0^3+\dfrac{1}{r_0}v_0^2\dfrac{\partial v_0}{\partial r_0} \end{array}\right]
+\upsilon\lambda_2\left[\begin{array}{l} u_0\dfrac{\partial^3 v_0}{\partial r_0\partial z_0^2}-2\dfrac{\partial v_0}{\partial z_0}\dfrac{\partial^2 w_0}{\partial z_0^2}+w_0\dfrac{\partial^3 v_0}{\partial z_0^3}-\dfrac{1}{r_0}\dfrac{\partial u_0}{\partial z_0}\dfrac{\partial v_0}{\partial z_0} \\ \quad +\dfrac{1}{r_0}v_0\dfrac{\partial^2 u_0}{\partial z_0^2}-\dfrac{\partial v_0}{\partial r_0}\dfrac{\partial^2 u_0}{\partial z_0^2}-\dfrac{\partial v_0}{\partial z_0}\dfrac{\partial^2 u_0}{\partial r_0\partial z_0}-\dfrac{1}{r_0}u_0\dfrac{\partial^2 v_0}{\partial z_0^2} \end{array}\right]. \tag{5}
$$

The conservation of energy is as follows:

$$
u_0\frac{\partial T_0}{\partial r_0}+w_0\frac{\partial T_0}{\partial z_0}=\alpha\frac{\partial^2 T_0}{\partial z_0^2}-\varepsilon_0\left[\begin{array}{l} u_0^2\dfrac{\partial^2 T_0}{\partial r_0^2}+2u_0w_0\dfrac{\partial^2 T_0}{\partial r_0\partial z_0}+w_0^2\dfrac{\partial^2 T_0}{\partial z_0^2}+u_0\dfrac{\partial w_0}{\partial r_0}\dfrac{\partial T_0}{\partial z_0} \\ \quad +u_0\dfrac{\partial u_0}{\partial r_0}\dfrac{\partial T_0}{\partial r_0}+w_0\dfrac{\partial u_0}{\partial z_0}\dfrac{\partial T_0}{\partial r_0}+w_0\dfrac{\partial w_0}{\partial z_0}\dfrac{\partial T_0}{\partial z_0} \end{array}\right]
+\frac{1}{\rho c_p}\frac{\partial}{\partial z_0}\left(\frac{16\sigma^* T_\infty^3}{3k^*}\frac{\partial T_0}{\partial z_0}\right)+q'''. \tag{6}
$$

The equations for species are as follows:

$$
u_0\frac{\partial a}{\partial r_0}+w_0\frac{\partial a}{\partial z_0}=D_A\frac{\partial^2 a}{\partial z_0^2}-k_c ab^2, \tag{7}
$$

$$
u_0\frac{\partial b}{\partial r_0}+w_0\frac{\partial b}{\partial z_0}=D_B\frac{\partial^2 b}{\partial z_0^2}+k_c ab^2. \tag{8}
$$

The relevant boundary conditions are as follows:

$$
\begin{aligned} &u_0=cr_0,\quad v_0=\Omega r_0,\quad w_0=0,\quad T_0=T_w,\quad D_A\frac{\partial a}{\partial z_0}=k_s a,\\ &D_B\frac{\partial b}{\partial z_0}=-k_s a\quad \text{at } z_0=0, \end{aligned} \tag{9}
$$

$$
u_0\to 0,\quad v_0\to 0,\quad T_0\to T_\infty,\quad a\to a_0,\quad b\to 0,\quad \text{as } z_0\to\infty. \tag{10}
$$

where u_0 suggests the velocity on r_0 direction and v_0, w_0 are the velocities on φ and z_0 directions, appropriately. Again σ^* is the Stefan–Boltzmann constant, λ_1 is the fluid relaxation time, λ_2 is the fluid retardation time, B_0 was the magnetic field strength, k^* is the mean absorption coefficient, T_0 is the fluid temperature, α is the thermal diffusivity, (k_c, k_s) are the rate constants, ϵ_0 is the thermal relaxation time and (D_A, D_B) are diffusion coefficients on species. This parameter on irregular heat source or sink q''' is as follows[6]:

$$q''' = \frac{k\Omega}{\upsilon}\left[\frac{A^*(T_w - T_\infty)}{\Omega r_0}u_0 + B^*(T - T_\infty)\right]. \tag{11}$$

By naturalizing von Karman as mentioned by Mogaji *et al.*,[40] we receive the following variables:

$$\begin{aligned} &\xi = \sqrt{\frac{\Omega}{\upsilon}}z_0, \quad u_0 = \Omega r_0 F, \quad v_0 = \Omega r_0 G,\\ &w_0 = \sqrt{\Omega\upsilon}H, \quad a = a_0\phi, \quad b = a_0 h, \quad \theta = \frac{T_0 - T_\infty}{T_w - T_\infty}. \end{aligned} \tag{12}$$

By renewing the conversion on Eqs. (3)–(8) and using Eq. (11), we acquire

$$2F + H' = 0, \tag{13}$$

$$\begin{aligned} &F'H + F^2 - G^2 - F'' + \beta_1(H^2F'' + 2HFF' - 2HGG')\\ &\quad + \beta_2(2F'^2 - F'''H + 2F'H'') + M(\beta_1 HF' + F) = 0, \end{aligned} \tag{14}$$

$$\begin{aligned} &G'H + 2FG - G'' + \beta_1(H^2G'' + 2(G'F + GF')H)\\ &\quad - \beta_2(HG''' - 2G'F' - 2H''G') + M(\beta_1 HG' + G) = 0, \end{aligned} \tag{15}$$

$$\left(1 + \frac{4}{3}\mathrm{Rd}\right)\frac{1}{\mathrm{Pr}}\theta'' - \theta'H - \varepsilon[\theta''H^2 + \theta'H'H] + A^*F + B^*\theta = 0, \tag{16}$$

$$\frac{1}{\mathrm{Sc}}\phi'' - \phi'H - k_1h^2\phi = 0, \tag{17}$$

$$\frac{\delta}{\mathrm{Sc}}h'' - h'H + k_1h^2\phi = 0. \tag{18}$$

These transformed boundary conditions were as follows:

$$\begin{aligned} &G(\xi) = 1, \quad F(\xi) = R, \quad H(\xi) = 0, \quad \theta(\xi) = 1, \quad \phi'(\xi) = k_2\phi(\xi),\\ &\delta h'(\xi) = -k_2\phi(\xi) \quad \text{at } \xi = 0, \end{aligned} \tag{19}$$

$$\begin{aligned} &G(\xi) \to 0, \quad F(\xi) \to 0, \quad \theta(\xi) \to 0, \quad \phi(\xi) \to 1,\\ &h(\xi) \to 0 \quad \text{as } \xi \to \infty, \end{aligned} \tag{20}$$

where we first display differentiation with respect to ξ. Again, $M(= \frac{\sigma B_0^2}{\rho\Omega})$ is the magnetic field parameter, $\beta_1 = (\lambda_1\Omega)$ is the time relaxation parameter, $R(= \frac{c}{\Omega})$ is the stretching parameter, $\beta_2 = (\lambda_2\Omega)$ is the retardation parameter, $\Pr(= \frac{\upsilon(\rho c_p)}{k})$ is the Prandtl number, $\varepsilon(= \varepsilon_0\Omega)$ is the thermal relaxation time, $\mathrm{Rd}(= \frac{4\sigma^* T_\infty^3}{kk^*})$ is the radiation parameter, $k_1(= k_c\frac{a_0^2}{\Omega})$ is the homogenous reaction rate, $\mathrm{Sc}(= \frac{\upsilon}{D_A})$ is the Schmidt number, $k_2(= \frac{k_s}{D_A}\sqrt{\frac{\upsilon}{\Omega}})$ is heterogeneous reaction rate, and $\delta(= \frac{D_B}{D_A})$ is the relation of diffusion coefficients. These species A^* and B^* are mostly not the same, yet they could await this to be related to size. They also studied the coefficients of diffusion species DB and DA that were exact, i.e. $\delta = 1$, so

$$\phi(\xi) + h(\xi) = 1. \tag{21}$$

Now applying the above condition, Eqs. (17) and (18) along with the corresponding boundary conditions give the pattern

$$\frac{1}{\mathrm{Sc}}\phi'' - \phi' H - k_1[1-\phi]^2\phi = 0, \tag{22}$$

$$\phi'(\xi) = k_2\phi(\xi) \quad \text{at } \xi = 0 \quad \text{and} \quad \phi(\xi) \to 1 \text{ as } \xi \to \infty. \tag{23}$$

These physical engineering parameters were detailed by the following equation:

$$\mathrm{Nu}_r = \frac{q_w}{k(T_w - T_\infty)}, \quad q_w = -\left[k\frac{\partial T_0}{\partial z_0} + q_r\right]_{z_0=0}. \tag{24}$$

As mentioned in Eq. (12), the non-dimensional system of local Nusselt number is as follows:

$$\mathrm{Nu}_r = -\left(1 + \frac{4}{3}\mathrm{Rd}\right)\theta'(0), \tag{25}$$

where $\mathrm{Re} = \frac{(\Omega r_0) r_0}{\upsilon}$ is the local Reynolds number.

3. Numerical Methods

The finite element method (FEM)[7,19,21] which is similar to the dominant technique discusses the ordinary and partial differential equations in a combined manner. This elementary concept of that technique was among the total domain with lesser elements by finite dimensions is called finite elements.

3.1. *The finite element method*

This FEM is an effective model for corrective PDEs and ODEs. This fundamental design of that process was the separation of the total domain with lesser elements by finite dimensions known as finite elements. That model was like the best numerical method in current engineering investigation, and it could be utilized on corrective integral equations as well as heat transfer, electrical systems, chemical processing, fluid mechanics and several more zones. The detailed steps using the finite element method are as follows:

(i) Finite element discretization

This total domain was separated with the finite number of sub-domains; this was known as the discretization on the domain. Every sub-domain was recognized as the element. This set of elements was recognized as the finite element coordinate.

(ii) Generation of the element equations

(a) Against the coordinate, the typical element was unique and the variational construction on the taken problems through the characteristic element was assembled.
(b) The relative outcome of that variational problem was affected, and the element equations were formed by substituting that result on the superior system.
(c) The element matrix, known as the stiffness matrix, was assembled by applying the element interruption functions.

(iii) Association of element equations

Every algebraic equation that was collected was constructed as commanding inter-element continuity conditions. The output of a high number of algebraic equations is called the universal finite element method; it conducts the total domain.

(iv) Obligation of conditions at boundary

This natural condition at the boundary is essentially required on the constructed equations.

(v) Solution of accumulated equations

These constructed equations that were much collected could be defined by every LU decomposition method, numerical techniques, especially, the Gauss elimination method, etc. The considerable study was to shape the functions that were occupied to exact existing applications.

Regarding the result on the order of nonlinear ordinary differential Eqs. (13)–(16) and (22) both into boundary conditions (19), (20) and (23), primarily, they accept

$$\frac{dF}{d\xi} = X, \tag{26}$$

$$\frac{dG}{d\xi} = Y. \tag{27}$$

Equations (13)–(16) and (22) then reduce to

$$2F + H' = 0, \tag{28}$$

$$\begin{aligned} &XH + F^2 - G^2 - X' + \beta_1(H^2X' + 2HFX - 2HGY) \\ &- \beta_2(2X^2 + X''H) + M(\beta_1 HX + F) = 0, \end{aligned} \tag{29}$$

$$\begin{aligned} &YH + 2FG - Y' + \beta_1(H^2Y' + 2(YF + GX)H) \\ &\quad - \beta_2(HY'' + 2XY) + M(\beta_1 HY + G) = 0, \end{aligned} \tag{30}$$

$$\left(1 + \frac{4}{3}\mathrm{Rd}\right)\frac{1}{\mathrm{Pr}}\theta'' - \theta' H - \varepsilon[\theta'' H^2 + \theta' H' H] + A^* F + B^* \theta = 0, \tag{31}$$

$$\frac{1}{\mathrm{Sc}}\phi'' - \phi' H - k_1[1 - \phi]^2\phi = 0. \tag{32}$$

3.2. *Variational formulation*

This variational pattern that is identical to Eqs. (28)–(32) through the typical linear element (ξ_b, ξ_{b+1}) is taken as follows:

$$\int_{\xi_b}^{\xi_{b+1}} w_1\left(\frac{dF}{d\xi} - X\right)d\xi = 0, \tag{33}$$

$$\int_{\xi_b}^{\xi_{b+1}} w_2\left(\frac{dG}{d\xi} - Y\right)d\xi = 0, \tag{34}$$

$$\int_{\xi_b}^{\xi_{b+1}} w_3(H' + 2F)d\xi = 0, \tag{35}$$

$$\int_{\xi_b}^{\xi_{b+1}} w_4\begin{pmatrix} XH + F^2 - G^2 - X' + \beta_1(H^2X' + 2HFX - 2HGY) \\ - \beta_2(2X^2 + X''H) + M(\beta_1 HX + F) \end{pmatrix}d\xi = 0, \tag{36}$$

$$\int_{\xi_b}^{\xi_{b+1}} w_5\begin{pmatrix} YH + 2FG - Y' + \beta_1(H^2Y' + 2(YF + GX)H) \\ - \beta_2(HY'' + 2XY) + M(\beta_1 HY + G) \end{pmatrix}d\xi = 0, \tag{37}$$

$$\int_{\xi_b}^{\xi_{b+1}} w_6\left(\left(1 + \frac{4}{3}\mathrm{Rd}\right)\frac{1}{\mathrm{Pr}}\theta'' - \theta' H - \varepsilon[\theta'' H^2 + \theta' H' H] + A^* F + B^* \theta\right)d\xi = 0, \tag{38}$$

$$\int_{\xi_b}^{\xi_{b+1}} w_7\left(\frac{1}{\mathrm{Sc}}\phi'' - \phi' H - k_1[1 - \phi]^2\phi\right)d\xi = 0, \tag{39}$$

where $w_1, w_2, w_3, w_5, w_6, w_4$ and w_7 are arbitrary test tasks and might been observed by the differences on F, G, H, X, Y, θ and ϕ, appropriately.

3.3. *Finite element formulation*

This finite element method might be constructed on the above equations that were replacing finite element approximations on this pattern

$$\begin{aligned} &X = \sum_{j=1}^{2} X_j\Omega_j, \quad Y = \sum_{j=1}^{2} Y_j\Omega_j, \quad \phi = \sum_{j=1}^{2} \phi_j\Omega_j, \quad F = \sum_{j=1}^{2} F_j\Omega_j, \\ &H = \sum_{j=1}^{2} H_j\Omega_j, \quad G = \sum_{j=1}^{2} G_j\Omega_j, \quad \theta = \sum_{j=1}^{2} \theta_j\Omega_j. \end{aligned} \tag{40}$$

$w_1 = w_2 = w_3 = w_4 = w_6 = w_7 = w_5 = \Omega_i, (i = 1, 2, 3, 4, 5, 6, 7)$. Here, Ω_i is the shape function of the typical element (ξ_b, ξ_{b+1}) and is denoted by

$$\begin{aligned} &\Omega_1^b = \frac{(\xi_{b+1} + \xi_b - 2\xi)(\xi_{b+1} - \xi)}{(\xi_{b+1} - \xi_b)^2}, \quad \Omega_2^b = \frac{4(\xi - \xi_b)(\xi_{b+1} - \xi)}{(\xi_{b+1} - \xi_b)^2}, \\ &\Omega_3^b = \frac{(\xi_{b+1} + \xi_b - 2\xi)(\xi - \xi_b)}{(\xi_{b+1} - \xi_b)^2}, \quad \xi_b \le \xi \le \xi_{b+1}. \end{aligned} \tag{41}$$

The finite element model on the equation so shaped is taken as follows:

$$\begin{bmatrix} [\Lambda^{11}] & [\Lambda^{12}] & [\Lambda^{13}] & [\Lambda^{14}] & [\Lambda^{15}] & [\Lambda^{16}] & [\Lambda^{17}] \\ [\Lambda^{21}] & [\Lambda^{22}] & [\Lambda^{23}] & [\Lambda^{24}] & [\Lambda^{25}] & [\Lambda^{26}] & [\Lambda^{27}] \\ [\Lambda^{31}] & [\Lambda^{32}] & [\Lambda^{33}] & [\Lambda^{34}] & [\Lambda^{35}] & [\Lambda^{36}] & [\Lambda^{37}] \\ [\Lambda^{41}] & [\Lambda^{42}] & [\Lambda^{43}] & [\Lambda^{44}] & [\Lambda^{45}] & [\Lambda^{46}] & [\Lambda^{47}] \\ [\Lambda^{51}] & [\Lambda^{52}] & [\Lambda^{53}] & [\Lambda^{54}] & [\Lambda^{55}] & [\Lambda^{56}] & [\Lambda^{57}] \\ [\Lambda^{61}] & [\Lambda^{62}] & [\Lambda^{63}] & [\Lambda^{64}] & [\Lambda^{65}] & [\Lambda^{66}] & [\Lambda^{67}] \\ [\Lambda^{71}] & [\Lambda^{72}] & [\Lambda^{73}] & [\Lambda^{74}] & [\Lambda^{75}] & [\Lambda^{76}] & [\Lambda^{77}] \end{bmatrix} \begin{bmatrix} F \\ G \\ H \\ X \\ Y \\ \theta \\ \phi \end{bmatrix} = \begin{bmatrix} \{r^1\} \\ \{r^2\} \\ \{r^3\} \\ \{r^4\} \\ \{r^5\} \\ \{r^6\} \\ \{r^7\} \end{bmatrix}, \tag{42}$$

where $[\Lambda^{mn}]$ and $[r^m]$ $(m, n = 1, 2, 3, 4, 5, 6, 7)$ was detailed by

$$\begin{aligned} &\Lambda^{11} = \int_{\xi_b}^{\xi_{b+1}} \Omega_i \frac{d\Omega_j}{d\xi} d\xi, \\ &\Lambda^{14} = -\int_{\xi_b}^{\xi_{b+1}} \Omega_i \Omega_j d\xi, \quad \Lambda^{12} = \Lambda^{13} = \Lambda^{15} = \Lambda^{16} = \Lambda^{17} = 0, \\ &\Lambda^{22} = \int_{\xi_b}^{\xi_{b+1}} \Omega_i \frac{d\Omega_j}{d\xi} d\xi, \quad \Lambda^{25} = -\int_{\xi_b}^{\xi_{b+1}} \Omega_i \Omega_j d\xi, \\ &\Lambda^{21} = \Lambda^{23} = \Lambda^{24} = \Lambda^{26} = \Lambda^{27} = 0, \\ &\Lambda^{33} = \int_{\xi_b}^{\xi_{b+1}} \Omega_i \frac{d\Omega_j}{d\xi} d\xi, \\ &\Lambda^{31} = 2\int_{\xi_b}^{\xi_{b+1}} \Omega_i \Omega_j d\xi, \quad \Lambda^{32} = \Lambda^{34} = \Lambda^{35} = \Lambda^{36} = \Lambda^{37} = 0, \end{aligned}$$

$$\begin{aligned} \Lambda^{44} = {} & \bar{H} \int_{\xi_b}^{\xi_{b+1}} \Omega_i \Omega_j d\xi - \int_{\xi_b}^{\xi_{b+1}} \Omega_i \frac{d\Omega_j}{d\xi} d\xi + \beta_1 \bar{H}^2 \int_{\xi_b}^{\xi_{b+1}} \Omega_i \frac{d\Omega_j}{d\xi} d\xi \\ & + 2\beta_1 \bar{H} \bar{F} \int_{\xi_b}^{\xi_{b+1}} \Omega_j \Omega_i d\xi - 2\beta_2 \bar{X} \int_{\xi_b}^{\xi_{b+1}} \Omega_j \Omega_i d\xi + \beta_2 \bar{H} \int_{\xi_b}^{\xi_{b+1}} \frac{d\Omega_i}{d\xi} \frac{d\Omega_j}{d\xi} d\xi \\ & + \beta_1 M \bar{H} \int_{\xi_b}^{\xi_{b+1}} \Omega_i \Omega_j d\xi, \Lambda^{41} = \bar{F} \int_{\xi_b}^{\xi_{b+1}} \Omega_i \Omega_j d\xi + M \int_{\xi_b}^{\xi_{b+1}} \Omega_i \Omega_j d\xi, \end{aligned}$$

$$\Lambda^{42} = -\bar{G} \int_{\xi_b}^{\xi_{b+1}} \Omega_i \Omega_j d\xi - 2\beta_1 \bar{X} \bar{Y} \int_{\xi_b}^{\xi_{b+1}} \Omega_i \Omega_j d\xi, \Lambda^{43} = \Lambda^{45} = \Lambda^{46} = \Lambda^{47} = 0,$$

$$
\begin{aligned}
\Lambda^{55} =& \bar{H}\int_{\xi_b}^{\xi_{b+1}} \Omega_i\Omega_j d\xi - \int_{\xi_b}^{\xi_{b+1}} \Omega_i \frac{d\Omega_j}{d\xi} d\xi + \beta_1 \bar{H}^2 \int_{\xi_b}^{\xi_{b+1}} \Omega_i \frac{d\Omega_j}{d\xi} d\xi + 2\beta_1 \bar{F}\bar{H} \\
&\times \int_{\xi_b}^{\xi_{b+1}} \Omega_i\Omega_j d\xi + \beta_2 \bar{H}\int_{\xi_b}^{\xi_{b+1}} \frac{d\Omega_i}{d\xi}\frac{d\Omega_j}{d\xi} d\xi - 2\beta_2 \bar{X}\int_{\xi_b}^{\xi_{b+1}} \Omega_i\Omega_j d\xi \\
&+ \beta_1 M\bar{H}\int_{\xi_b}^{\xi_{b+1}} \Omega_i\Omega_j d\xi, \\
\Lambda^{52} =& 2\bar{F}\int_{\xi_b}^{\xi_{b+1}} \Omega_i\Omega_j d\xi + M\int_{\xi_b}^{\xi_{b+1}} \Omega_i\Omega_j d\xi, \\
\Lambda^{54} =& 2\beta_1 \bar{G}\bar{H}\int_{\xi_b}^{\xi_{b+1}} \Omega_i\Omega_j d\xi, \Lambda^{51} = \Lambda^{53} = \Lambda^{56} = \Lambda^{57} = 0, \\
\Lambda^{66} =& -\left(1+\frac{4}{3}\mathrm{Rd}\right)\frac{1}{\mathrm{Pr}}\int_{\xi_b}^{\xi_{b+1}} \frac{d\Omega_i}{d\xi}\frac{d\Omega_j}{d\xi} d\xi - \bar{H}\int_{\xi_b}^{\xi_{b+1}} \Omega_i \frac{d\Omega_j}{d\xi} d\xi + \varepsilon\bar{H}^2\int_{\xi_b}^{\xi_{b+1}} \\
&\times \frac{d\Omega_i}{d\xi}\frac{d\Omega_j}{d\xi} d\xi - \varepsilon\bar{H}\bar{H}'\int_{\xi_b}^{\xi_{b+1}} \Omega_i \frac{d\Omega_j}{d\xi} d\xi + B^*\int_{\xi_b}^{\xi_{b+1}} \Omega_i\Omega_j d\xi, \\
\Lambda^{61} =& A^*\int_{\xi_b}^{\xi_{b+1}} \Omega_i\Omega_j d\xi, \Lambda^{62} = \Lambda^{63} = \Lambda^{64} = \Lambda^{65} = \Lambda^{67} = 0, \\
\Lambda^{77} =& -\frac{1}{\mathrm{Sc}}\int_{\xi_b}^{\xi_{b+1}} \frac{d\Omega_j}{d\xi}\frac{d\Omega_i}{d\xi} d\xi - \bar{H}\int_{\xi_b}^{\xi_{b+1}} \Omega_i \frac{d\Omega_j}{d\xi} d\xi - k_1[1-\bar{\phi}]^2\int_{\xi_b}^{\xi_{b+1}} \Omega_i\Omega_j d\xi, \\
\Lambda^{71} =& \Lambda^{72} = \Lambda^{73} = \Lambda^{74} = \Lambda^{75} = \Lambda^{76} = 0,
\end{aligned}
$$

$$
\begin{aligned}
b^1 &= b^2 = b^3 = 0, \quad b^4 = \beta_2\bar{H}\left(\Omega_i\frac{dX}{d\xi}\right)_{\xi_b}^{\xi_{b+1}}, \quad b^5 = \beta_2\bar{H}\left(\Omega_i\frac{dY}{d\xi}\right)_{\xi_b}^{\xi_{b+1}}, \\
b^6 &= -\left(1+\frac{4}{3}\mathrm{Rd}\right)\frac{1}{\mathrm{Pr}}\left(\Omega_i\frac{d\theta}{d\xi}\right)_{\xi_b}^{\xi_{b+1}} + \varepsilon\bar{H}^2\left(\Omega_i\frac{d\theta}{d\xi}\right)_{\xi_b}^{\xi_{b+1}}, \\
b^7 &= -\frac{1}{\mathrm{Sc}}\left(\Omega_i\frac{d\phi}{d\xi}\right)_{\xi_b}^{\xi_{b+1}}.
\end{aligned}
$$

3.4. *Validation of numerical scheme*

Table 1 is the calculation table on $F'(0), -G'(0)$ and $-\theta'(0)$ is the absence of fluid parameters into correlation in a few previously issued appliances. Definitely, in this

Table 1. A correlation on $F'(0), -G'(0)$ and $-\theta'(0)$ of fixed $\mathrm{Pr} = 6.2$ and $\beta_1 = 0 = \beta_2 = M = R = \varepsilon = \mathrm{Rd} = A^* = B^*$.

	Turkyilmazoglu[17]	Bachok *et al.*[18]	Hafeez *et al.*[4]	Present
$-G'(0)$	0.6159220	0.6159	0.6158492796	0.6159284093
$F'(0)$	0.51023262	0.5102	0.5101162643	0.5102336183
$-\theta'(0)$	0.93387794	0.9337	0.9336941128	0.9338715627

table, the new analysis is numerical and authentically designs the finite element method which is the accurate technique.

4. Results and Discussion

In the analysis, the main ambition was to anticipate the physics of thermal-radiated Oldroyd-B fluid flow inferior to the changed Fourier's law and investigate it numerically. We have utilized the finite element method to detect the analysis of physical behavior by numerous parameters. The physical effect on many parameters of flow, solutal distributions and temperature was marked and sketched in Figs. 2–12. Fixed values are distributed over total leading parameters as the numerical imitations such as $\beta_1 = 0.1, \mathrm{Pr} = 2.5, \beta_2 = 0.1, M = 0.1, \varepsilon = 0.3, \mathrm{Sc} = 5.0, k_1 = 0.1, R = 0.8, k_2 = 0.1, A^* = 0.2$, $B^* = 0.01$ and $\mathrm{Rd} = 0.1$ and some are mentioned in graphs. This was observed in total plots that were asymptotically coming from the far-field boundary conditions. It gathered information about the issue based on specific physical factors on the ranges $0.1 \le \beta_1 \le 0.4$, $0.1 \le \beta_2 \le 0.25$, $0.2 \le \varepsilon \le 0.35$, $0.05 \le \mathrm{Rd} \le 0.35$, $-4.0 \le A^* \le 4.0$, $-0.2 \le B^* \le 0.04$, $0.1 \le k_1 \le 0.5$, and $0.2 \le k_2 \le 0.6$.

The curves of velocity components like radial $F(\xi)$, tangential $G(\xi)$, axial $-H(\xi)$ and temperature $\theta(\xi)$, respectively, were plotted in Figs. 2–5 against the varying values of β_1. Figure 2 discovers the variation of radial velocity $F(\xi)$ from the relaxation time factor β_1. They show the velocity of the forward radial direction downturn as given by the relaxation time parameter β_1 in the range 0.1–0.4. By that time, the material ratio for both relaxation time and material inspection time will be received. Hence, their greater assessment of the relaxation time factor assumes that the stress relaxation was higher or that inspection time was lesser, indicating this

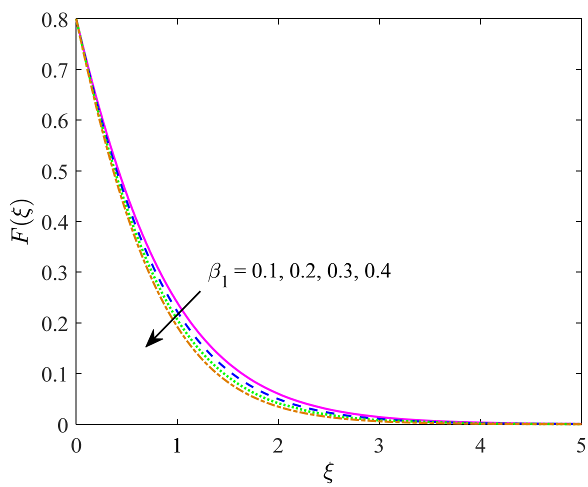

Fig. 2. (Color online) Impression on β_1 of $F(\xi)$.

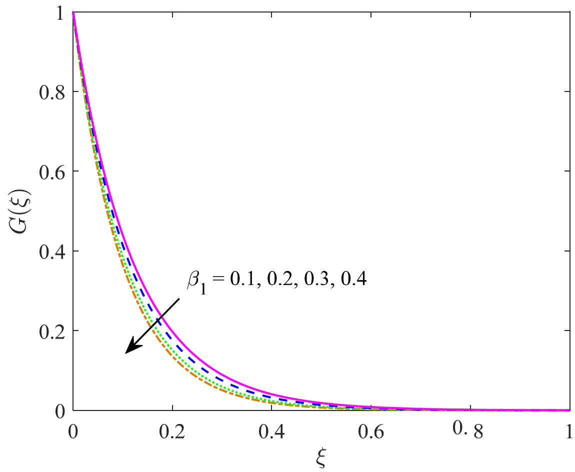

Fig. 3. (Color online) Impression of β_1 on $G(\xi)$.

fluid displays a solid-like response. So, the fluid was loaded in extra protection. Accordingly, the velocity of the fluid reduces in that manner. This equal position on the flow act could be noticed in the azimuthal direction via Fig. 3. Furthermore, an important decline was seen in the viscosity of boundary layer. This velocity field in the axial direction is displayed in Fig. 4. It was noticed that velocity distribution on the axial direction was reduced as an effect on $\beta_1(= 0.1, 0.2, 0.3, 0.4)$. The behavior of temperature distribution $\theta(\xi)$ to the liquid is shown in Fig. 5. Through later examination, they discover that the fluid temperature $\theta(\xi)$ improves the augmentation on $\beta_1(= 0.1, 0.2, 0.3, 0.4)$. Physically, this could be interpreted by the impact on the Deborah number of relaxation time into the fluid that acts as the solid-like reaction.

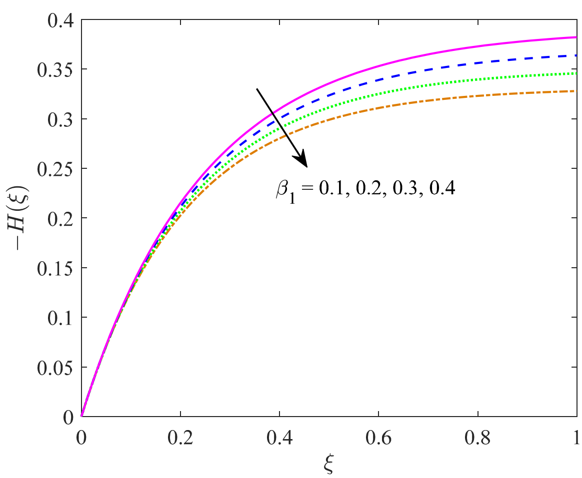

Fig. 4. (Color online) Impression of β_1 on $-H(\xi)$.

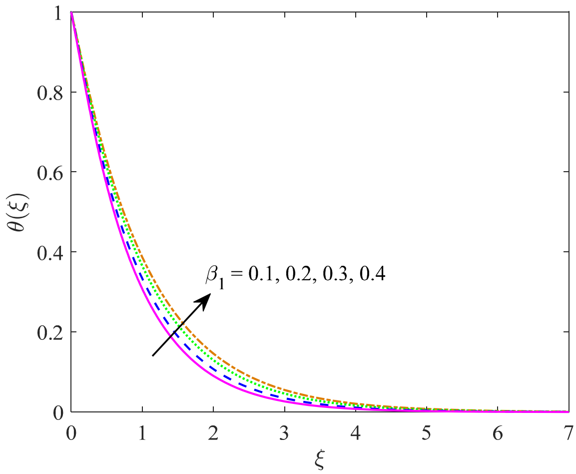

Fig. 5. (Color online) Impression of β_1 on $\theta(\xi)$.

Because of every conductive heat transport that improves on solid-like fluid by being related to a liquid, hence, this temperature increases in that position. A similar observation was found by Hafeez *et al.*[4] and Elanchezhian *et al.*[5]

The distinction between velocity field and temperature distribution from the retardation time factor, β_2, is shown in Figs. 6 and 7. The impact on β_2 of velocity profile $G(\xi)$ in the azimuthal direction is definite in Fig. 6. It is noticed from curves of that design that the magnitude of velocity $G(\xi)$ on azimuthal direction improves the ascent of the retardation time parameter β_2. The retardation time depicts the time taken to form the shear stress on the fluid. Hence it could describe time-scales when the association picture is not interpreted with the relaxation time. This function $G(\xi)$

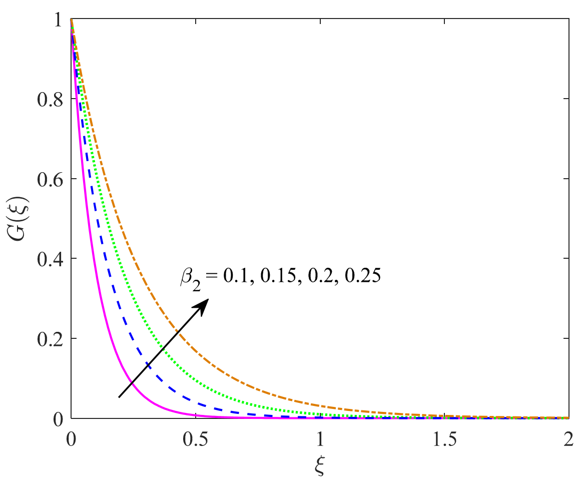

Fig. 6. (Color online) Impression of β_2 on $G(\xi)$.

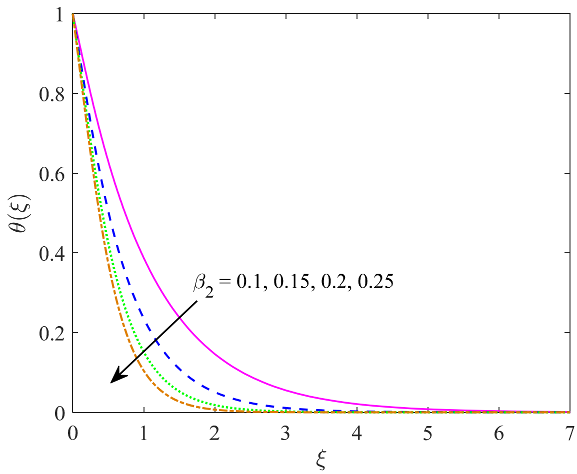

Fig. 7. (Color online) Impression of β_2 on $\theta(\xi)$.

was directly compared to retardation time parameter β_2. This represents that the fluid flow was parallel toward the disk and expedited at a greater rate during fluid relaxation time. Figure 7 explains the effect of temperature on the fluid for changeable values of $\beta_2 = (0.1, 0.15, 0.2, 0.25)$ as observance defect parameters fixed. They were located at the temperature $\theta(\xi)$ that was decelerated below the activity on the retardation time parameter β_2. This greater retardation time β_2 raises the elasticity on the fluid. As a result of that behavior, a decreasing function of $\theta(\xi)$ was acclaimed. Previous investigation[5] got the similar behavior.

The impact on thermal relaxation time ε and radiation parameter Rd in temperature $\theta(\xi)$ is shown in Fig. 8 with the other parameters taken as fixed.

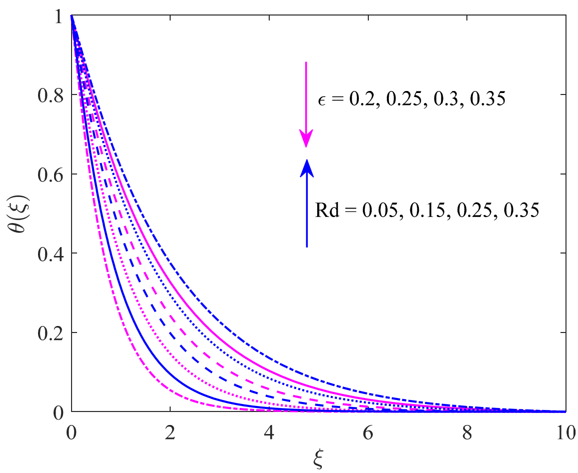

Fig. 8. (Color online) Impression on ε and Rd of $\theta(\xi)$.

The thermal relaxation time has increased from $\varepsilon(= 0.2, 0.25, 0.3, 0.35)$. That was the reduction performance at the temperature of the Oldroyd-B fluid. Actually, about $\varepsilon = 0.0$, Cattaneo–Christov figure reduction is seen in the classical Fourier's law that represents the energy of heat transport instantly on the fluid. On the other hand, increase in nonzero values on ε decreases temperature distribution. As a result of the non-Fourier heat flux model, the command to rate of heat energy was taken on a liquid.

This impact on radiation parameter Rd on the distribution of temperature $\theta(\xi)$ is also examined in Fig. 8. Against this sketch, it was observed that the consequence on Rd on $\theta(\xi)$ was developing. It was simple as the radiation mechanism was the heat transference aspect that discharged the power by liquid particles just like the few added heats that were composed on the flow. Thus, they exposed the enhancement on the thermal field about greater $\mathrm{Rd}(= 0.05, 0.15, 0.25, 0.35)$. A similar pattern was observed by Anantha Kumar *et al.*[25]

The influence on heat fall/rise factor in temperature profile $\theta(\xi)$ had been calculated on Fig. 9. It could be analyzed to the $\theta(\xi)$ was increasing with the dimensionless same as variable ξ about the growing values of space and temperature reliant on heat rise/sink parameters (A^*B^*). Actually, they could be announced by, positive ness of A^* and B^* indicate into the heat source that execute such heat generators when that heat energy had been discharged against the flow and that details increase on temperature field. This negativity of A^* and B^* express by heat sink that performs by heat absorbers, this energy was consumed about unfavorable values of A^* and B^*.

Figure 10 shows the impact of homogeneous strength k_1 and heterogeneous strength k_2 on concentration distribution $\phi(\xi)$ with other parameters fixed. It is seen that the concentration field decreases in the extended raises on the homogeneous reaction parameter k_1. This was the reason the diffusion coefficients were affected by

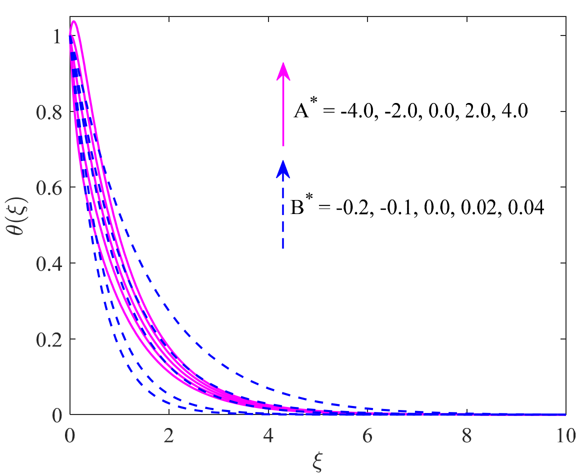

Fig. 9. (Color online) Impression of A^* and B^* on $\theta(\xi)$.

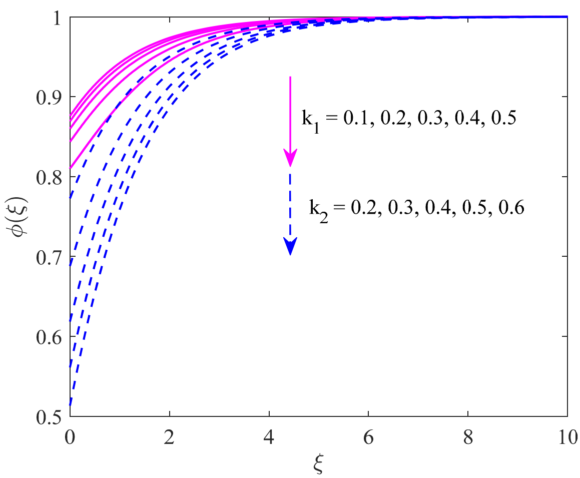

Fig. 10. (Color online) Impression on k_1 and k_2 of $\phi(\xi)$.

the reaction rates. It was also noted that the effect on heterogeneous reaction parameter k_2 was to decrease the species concentration. The raise on the heterogeneous power details reduces the diffusion of concentration. Due to that reason, the concentration distribution was reduced in the increasing values of k_2.

The behaviors of space and temperature that were reliant on the heat rise/sink parameter in the Nusselt number were displayed in Fig. 11. It is noted that heat transfer is initially increasing and then the decreasing behavior is noted for incremental values of A^*. Further, the rate of heat transfer was decreased about greater values of B^*. In Fig. 12, the alteration of concentration gradient by the wall $-\phi'(0)$ in different physical factors was considered. It was clearly noted that the greater values of k_1 and k_2 display a developing trend of wall concentration gradient.

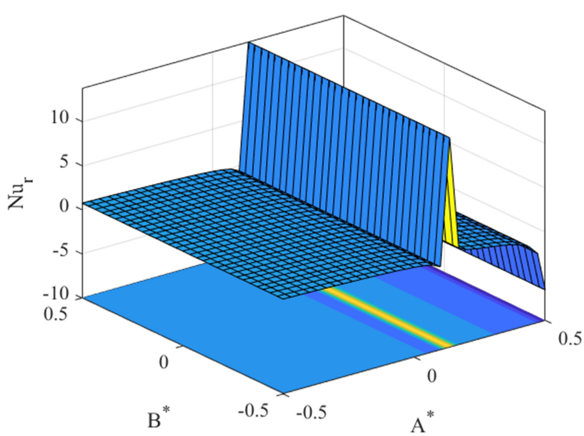

Fig. 11. (Color online) Impression on A^* and B^* of Nu_r.

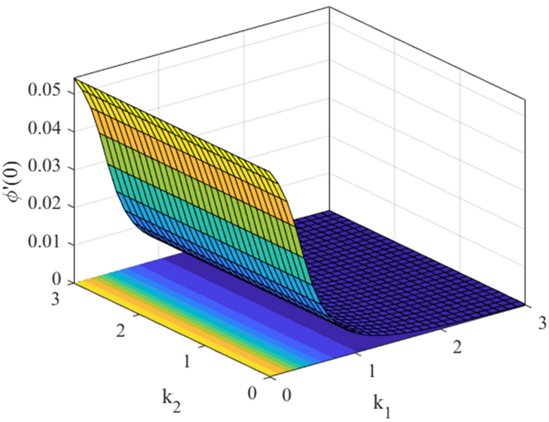

Fig. 12. (Color online) Impression on k_1 and k_2 of Nu_r.

The analytical path (slope of linear regression by data points) had been applied to evaluate the raise/reduce on Nu_r about different values on governing parameters; see Table 2. In Table 2, numerical values of Nu_r regarding the variation of $\beta_2, \mathrm{Pr}, R, \varepsilon$ and Rd are presented. The data have shown an increase at the rate 0.031498 for

Table 2. Numerical computations by local Nusselt number for different physical parameters.

β_2	Pr	R	ϵ	Rd	Nu_r
0.1	0.71	0.5	0.1	0.1	0.12078857
0.2					0.16164530
0.3					0.20966892
0.4					0.26215527
Slope					**0.472124**
	0.5				0.11775037
	1.0				0.12647360
	1.5				0.14147399
	2.0				0.16524620
	Slope				**0.031498**
		0.6			0.12856569
		1.0			0.16271023
		1.4			0.20126210
		1.8			0.24356004
		Slope			**0.095884**
			0.0		0.12015519
			0.2		0.12154809
			0.4		0.12361662
			0.6		0.12693212
			Slope		**0.0112**
				0.0	0.10803495
				0.2	0.13368504
				0.4	0.15973808
				0.6	0.18599496
				Slope	**0.129967**

larger values of Pr. As developing Pr causes reduction in the temperature, this was done on the sense of Prandtl number that was related into thermal diffusivities and the momentum and into the augmentation on the Prandtl number that the advantage toward the reduction on the thermal diffusivity and when that temperature reduces. Due to this reason, the rate of heat transfer accelerates. Here also, Nu_r increases at the rates $0.472124, 0.095884, 0.0112$ and 0.129967 with an enhancement in the magnitude of β_2, R, ε and Rd correspondingly.

5. Conclusion

This present analysis was committed toward examining the three-dimensional Oldroyd-B fluid into the effect on homogeneous–heterogeneous reactions, where the fluid flows through the rotating disk. Further, a changed Fourier's law model was applied for this study. The impacts on temperature and space reliant on heat source/sink and thermal radiation were analyzed. The PDEs were transformed into ODEs with the aid of applicable comparison conversion. Recently, the determined outcomes that were collected against the finite element method and the previous results were studied. The additional tabular comparison and graphical representation approve that the finite element method was exactly usable for like problems and several others. This technique could be more favorable than other nonlinear problems. Thus, the basic points of the present analysis are as follows:

(1) Reducing acts on azimuthal velocity and radial velocity were observed on the relaxation time parameter.
(2) This was noticed for those greater values of retardation parameter and fluid relaxation time parameter which cause enhancement in temperature distribution.
(3) These azimuthal velocity sketches were raising applications on the retardation time factor.
(4) Thermal retardation time parameter and relaxation time parameter increase under the fluid temperature.
(5) The temperature was affected by the increasing temperature and space-related heat source or sink factors (A^*, B^*) and heat transfer was increased by escalation on the Prandtl number.
(6) Devaluation into the concentration field was noticed although influences on homogeneous and heterogeneous reactions become greater.

The present nature was also higher to the region of cooling on nuclear reactors, food products were collected in the path of the surrounding environment over the food and space technology, the resonance of organs along with tumors into medical fields such as cancer therapy and magnetic resonance imaging and several more. In further studies, the present model will extend bioconvection in motile microorganisms.

Acknowledgment

We are very grateful to the editor and reviewers for their constructive suggestions.

ORCID

M. Rupa Lavanya https://orcid.org/0000-0002-8040-0607
Kotha Gangadhar https://orcid.org/0000-0002-0264-2512
D. Naga Bhargavi https://orcid.org/0000-0003-2522-0715
Ali J. Chamkha https://orcid.org/0000-0002-8335-3121

References

1. T. Von Karman, *Z. Angew Math. Mech.* **1** (1921) 233.
2. W. G. Cochran, *Math. Proc. Camb. Philos. Soc.* **30**(3) (1934) 365.
3. E. R. Benton, *J. Fluid Mech.* **24**(4) (1966) 781.
4. A. Hafeez, M. Khan and J. Ahmed, *J. Therm. Anal. Calorim.* **144** (2021) 793.
5. E. Elanchezhian, R. Nirmalkumar, M. Balamurugan, K. Mohana, K. M. Prabu and A. Viloria, *J. Therm. Anal. Calorim.* **141** (2020) 2613.
6. Usman, P. Lin and A. Ghafari, *J. Therm. Anal. Calorim.* **146** (2021) 1735.
7. S. O. Alharbi, *J. Therm. Anal. Calorim.* **145** (2021) 161.
8. J. B. J. Fourier, *Théorie Analytique De La Chaleur* (Acadéemie des Sciences, Paris, 1822).
9. C. Cattaneo, *Atti Semin. Mat. Fis. Univ. Modena Reggio Emilia* **3** (1948) 83.
10. C. I. Christov, *Mech. Res. Commun.* **36** (2009) 481.
11. M. Ciarletta and B. Straughan, *Mech. Res. Commun.* **37** (2010) 445.
12. K. Z. Zhang, N. A. Shah, D. Vieru and E. R. El-Zahar, *Int. Commun. Heat Mass Transf.* **135** (2022) 106138.
13. I. Ahmad, M. Faisal, T. Javed and I. L. Animasaun, *Ain Shams Eng. J.* **13**(1) (2022) 101494.
14. A. M. Alsharif, A. I. Abdellateef, Y. A. Elmaboud and S. I. Abdelsalam, *Appl. Math. Mech.-Engl. Ed.* **43** (2022) 931.
15. M. A. Chaudhary and J. H. Merkin, *Fluid Dyn. Res.* **16** (1995) 311.
16. J. H. Merkin, *Math. Comput. Model.* **24** (1996) 125.
17. M. Turkyilmazoglu, *Comput. Fluids* **94** (2014) 139.
18. N. Bachok, A. Ishak and I. Pop, *Phys. B: Condens. Matter* **406** (2011) 1767.
19. P. Sreedevi, P. Sudarsana Reddy and M. A. Sheremet, *J. Therm. Anal. Calorim.* **141** (2020) 533.
20. M. Javed, F. Qadeer, N. Imran, P. Kumam and M. Sohail, *Alex. Eng. J.* **61**(12) (2022) 10677.
21. A. Almaneea, *Alex. Eng. J.* **61**(10) (2022) 8343.
22. B. K. Siddiqui, S. Batool, Q. Hussan and M. Y. Malik, *Ain Shams Eng. J.* **13**(1) (2022) 101493.
23. N. S. Khashi'ie, N. M. Arifin, N. C. Rosca, A. V. Rosca and I. Pop, *Int. J. Numer. Method Heat Fluid Flow* **32**(2) (2022) 568.
24. N. A. L. Aladdin and N. Bachok, *Int. J. Numer. Method Heat Fluid Flow* **32**(2) (2022) 660.
25. K. Anantha Kumar, N. Sandeep, V. Sugunamma and I. L. Animasaun, *J. Therm. Anal. Calorim.* **139** (2020) 2145.
26. A. Rauf, Faisal and T. Mushtaq, *Appl. Nanosci.* **12** (2022) 2059.

27. M. Luo, C. Wang, J. Zhao and L. Liu, *Int. J. Heat Mass Transf.* **188** (2022) 122597.
28. P. Rana, S. Gupta and G. Gupta, *Int. Commun. Heat Mass Transf.* **134** (2022) 106025.
29. M. Hussain, U. Farooq and M. Sheremet, *Int. Commun. Heat Mass Transf.* **137** (2022) 106230.
30. K. Sharma, N. Vijay, F. Mabood and I. A. Badruddin, *Int. Commun. Heat Mass Transf.* **133** (2022) 105977.
31. N. Vijay and K. Sharma, *Chin. J. Phys.* **78** (2022) 83.
32. S. Kumar and K. Sharma, *Chin. J. Phys.* **77** (2022) 861.
33. K. Gangadhar, P. Manasa Seshakumari, M. Venkata Subba Rao and A. J. Chamkha, *Proc. IMechE Part E: J. Process Mech. Eng.* **236**(4) (2022) 1661.
34. N. A. Zainal, R. Nazar, K. Naganthran and I. Pop, *Int. J. Numer. Methods Heat Fluid Flow* **32**(8) (2022) 2640.
35. Y. Bai, H. Fang and Y. Zhang, *Int. J. Numer. Methods Heat Fluid Flow* **32**(6) (2022) 2198.
36. K. Venkata Ramana, K. Gangadhar, T. Kannan and A. J. Chamkha, *J. Therm. Anal. Calorim.* **147** (2022) 2749.
37. K. Gangadhar, M. Venkata Subba Rao, S. Kumar, S. Sharma and S. R. Munjam, *Int. J. Ambient Energy* **43**(1) (2022) 1345.
38. M. Ibrahim, T. Saeed and S. Zeb, *Eur. Phys. J. Plus* **137** (2022) 609.
39. M. Ibrahim, S. Ahmad, T. Saeed and S. Zeb, *Eur. Phys. J. Plus* **137** (2022) 766.
40. T. S. Mogaji, A. O. Olapojoye, E. T. Idowu and B. Saleh, *J. Braz. Soc. Mech. Sci. Eng.* **44** (2022) 90.